Controllable Stearic Acid Crystal Induced High Hydrophobicity on Cellulose Film Surface

Meng He,[†] Min Xu,[‡] and Lina Zhang*[,†]

[†]Department of Chemistry, Wuhan University, Wuhan 430072, China

[‡]Shanghai Key Laboratory of Magnetic Resonance, Department of Physics, East China Normal University, Shanghai 200062, China

S *Supporting Information*

ABSTRACT: A novel, highly hydrophobic cellulose composite film (RCS) with biodegradability was fabricated via solvent-vaporized controllable crystallization of stearic acid in the porous structure of cellulose films (RC). The interface structure and properties of the composite films were investigated with wide-angle X-ray diffraction (WAXD), scanning electron microscopy (SEM), differential scanning calorimetry (DSC), FT-IR, solid-state ^{13}C NMR, water uptake, tensile testing, water contact angle, and biodegradation tests. The results indicated that the RCS films exhibited high hydrophobicity (water contact angle achieved to 145°), better mechanical properties in the humid state and lower water uptake ratio than RC. Interestingly, the stearic acid crystallization was induced by the pore wall of the cellulose matrix to form a micronano binary structure, resulting in a rough surface. The rough surface with a hierarchical structure containing micronanospace on the RCS film surface could trap abundant air, leading to the high hydrophobicity. Moreover, the RCS films were flexible, biodegradable, and low-cost, showing potential applications in biodegradable water-proof packaging.

KEYWORDS: *high-hydrophobic cellulose film, controllable crystallization, interface structure, biodegradable, waterproof, packaging material*
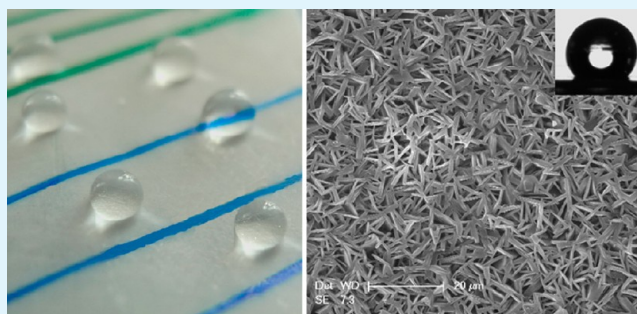
1. INTRODUCTION

Recently, the eco-friendly and biodegradable natural polymers for various applications have received much attention, as a result of increased worldwide concern about sustainability issues.[1,2] However, most natural polymers such as cellulose and chitin are difficult to dissolve, which restricts their application. In our laboratory, novel green solvent systems, such as NaOH/urea aqueous solution with cooling, have been developed to dissolve the most intransigent macromolecules such as cellulose and chitin.[3,4] Cellulose is the most abundant renewable biopolymer and can be converted into regenerated materials (films, microspheres, hydrogels, scaffold, and fibers).[5−8] Moreover, the regenerated cellulose films have the potential to replace some petroleum-based plastics due to its low-cost, transparency, good mechanical properties, and biodegradability.[5] However, the regenerated cellulose film shows poor water resistance properties. It is, therefore, essential to improve the hydrophobicity of the cellulose films for further commercial applications. There are several ways to improve the surface hydrophobicity such as a hierarchical micro/nanostructure and low-surface-energy materials combination,[9] network structure or porous nanostructures formation,[10,11] and a rough surface induced by crystallization control.[12,13] Stearic acid, a saturated fatty acid derived from animal and vegetable fats and oils, can be used in the field of moisture barrier[14] and cellulose fiber dispersion[15] due to its low surface energy,[16] inertness, low cost,

low toxicity, and biocompatibility.[17] As a component of wax used by nature to create superhydrophobic lotus leaves,[16,18] stearic acid has been incorporated into a hydroxyl propyl methyl cellulose (HPMC) based film[19] and zein sheets for a moisture barrier[14] and has been used for modifying soy protein isolate as environment-friendly "green" plastics.[20] To the best of our knowledge, hydrophobic modification of cellulose materials mainly includes constructing special morphologies,[21,22] gas phase surface etherification[23] C$_{14}$-graft,[24] and sol−gel coating of decyltrimethoxysilane (DTMS) as well as tetraethylorthosilicate (TEOS).[25] Additionally, standard hydrophilic cellulose papers with superhydrophobic surfaces have been prepared using plasma processing techniques,[26] and cellulose fibers have been modified or treated to improve the hydrophobicity.[27−30]

It is known that the water repellency of the surface can be dramatically enhanced by increasing the surface roughness to mimic the natural-occurring hydrophobic leaves or insects such as lotus leaves and water strider legs.[31,32] The colloid deposition method can be used widely to yield nanostructured rough surfaces for the hydrophobicity improvement[33,34] and oil−water separation[35] very recently. However, this method usually

requires harsh conditions such as high temperature,[35] which is unsuitable for ordinary polymers. The solvent vaporization or solvent diffusion inducing crystallization can also construct the rough structure to lead the superhydrophobic surface in relatively mild conditions.[36,12,13] In this work, a simple and "green" method for preparation of the high-hydrophobic cellulose films was presented and their structure and properties were investigated. Cellulose/stearic acid composite gel sheets were prepared first and then hot-pressed to fabricate cellulose/stearic acid films, which was very different from HPMC/stearic acid film preparation by adding stearic acid into the HPMC solution.[19] The controllable stearic acid crystallization in micropores of the regenerated cellulose film surface and interface can lead to high hydrophobicity through construction of the rough surface structure. The major goal of this work was to prepare a cellulose film with hydrophobicity and biodegradability, hoping to broaden the applications of cellulose in the waterproof package field.

2. EXPERIMENTAL SECTION

2.1. Materials. The cellulose sample (cotton linter pulp) was supplied by Hubei Chemical Fiber Co. Ltd. (Xiangfan, China). Its viscosity-average molecular weight (M_η) was determined by using an Ubbelohde viscometer in a LiOH/urea aqueous solution at 25 ± 0.05 °C and calculated from the equation $[\eta] = 3.72 \times 10^{-2} M_w^{0.77}$ to be 10.0×10^4 g/mol.[37] The stearic acid, NaOH, Span-80, ethanol and urea were of analytical grade and used without further purification. Copy paper (Jin Guang Co. Ltd., China) and thermal paper (PLUS, Japan) were bought and used directly.

2.2. Preparation of Cellulose/Stearic Acid Composite Films. In total, 7 wt % NaOH and 12 wt % urea aqueous solution were precooled to −12.8 °C, and then the desired amounts of cellulose sample were added immediately. The cellulose was completely dissolved within 5 min with a stirring speed at about 1800 rpm to obtain a transparent solution. The resultant cellulose solution was centrifuged to degas at 6000 rpm for 15 min and then cast on a glass plate to provide a gel sheet with the thickness of about 0.2 mm. Subsequently, it was immediately coagulated with a 5 wt % H_2SO_4 and 10 wt % Na_2SO_4 aqueous solution for 15 min to obtain cellulose gel sheets, and then the gel sheets were washed exhaustively with deionized water to remove the residual urea and NaOH. Moreover, the gel sheets were soaked in stearic acid/ethanol solutions of different concentrations for 15 min with stirring and then hot-pressed at 90 and 100 °C, respectively, with about 0.1 MPa stress to fabricate the regenerated cellulose films embedded with stearic acid (RCS), as shown in Scheme 1. The RCS composite films were coded as RCS1, RCS3, RCS5, RCS20, and RCS40, according to the concentrations of stearic acid (1, 3, 5, 20, 40 g/100 mL, respectively). The pure regenerated cellulose film was coded as RC.

2.3. Characterization. Scanning electron microscopy (SEM) observation was carried out with a Hitachi X-650 microscope (Mountain View, CA, Japan) and FESEM (SIRION TMP, FEI). The films were frozen in liquid nitrogen, immediately snapped, and then freeze-dried for the SEM observation. The surface of the films (freezing or hot-pressing dried) was sputtered with platinum and then observed. Wide angle X-ray diffraction measurements were measured with a WAXD diffractometer (D8-Advance, Bruker). The patterns with Cu K$_\alpha$ radiation ($\lambda = 0.154\,06$ nm) at 40 kV and 30 mA were recorded in the region of 2θ from 4 to 40°. The samples were cut into powder and dried in a vacuum oven for 48 h before testing. FT-IR spectra were carried out with a FT-IR spectrometer (1600, Perkin−Elmer Co., MA) in the wavelength range from 4000 to 400 cm^{-1}. The powdered and vacuum-dried samples were obtained, and the test specimens were prepared by the KBr disk method. Solid-state ^{13}C NMR spectra of dried samples were recorded on a Bruker AVANCE III spectrometer operated at a ^{13}C frequency of 75 MHz using the combined technique of magic angle spinning (MAS) and cross-

Scheme 1. Preparation Process of RCS Films[a]
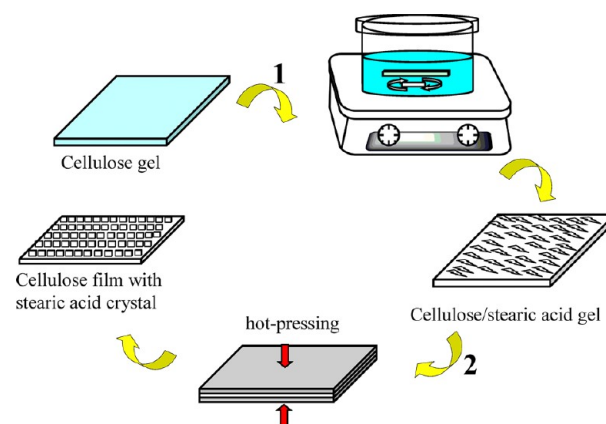
[a](1) Soaking in the stearic acid/ethanol solution at 60 °C with stirring; (2) hot-pressing at 90 and 100 °C.

polarization. The spinning speed was set at 5 kHz for all samples. The contact time was 3 ms, the acquisition time 50 ms, and the recycle delay 3 s. A typical number of 1024 scans were acquired for each spectrum. Differential scanning calorimetry (DSC) experiments were performed on a NETZSCH DSC 200PC (NETZSCH, Germany) with a heating rate of 5 °C/min. The temperature was controlled with liquid nitrogen, and the dried samples were put in a tightly sealed aluminum cell.

Water contact angle was measured and calculated in dynamic mode on a Data Physics Instrument (OCA20). One drop of water (2 μL) was put on the surface of the films with an automatic piston syringe and photographed. For the water uptake test, the RCS and RC films were preconditioned at 60 °C for 24 h and weighed (W_0). After immersing in distilled water for an expected time, the films were blotted with filter paper towels to remove the excess water carefully on the surface and weighed (W_t). The water uptake ratio was calculated according to eq 1 as follows:

$$\text{water uptake}(\%) = \frac{W_t - W_0}{W_0} \times 100 \tag{1}$$

The mechanical properties of the films in the dry and humid states were measured on a universal tensile tester (CMT 6503, Shenzhen SANS Test Machine Co. Ltd., Shenzhen, China) according to ISO527-3-1995 (E) at a speed of 2 mm/min^{-1}. The films (at 97.5% humidity) were kept in the container with saturated saline solution (K_2SO_4) at 25 °C for 48 h before the test. Because the strength data are related to the environmental temperature and humidity, all measurements were made under the same conditions. The mung beans were used to test the water resistant properties as package material for RC and RCS20. In the test, the RC and RCS20 films were used for the bottom of the vessels, and the bottom was immersed in water merely. The mung beans were put on the films at 25 °C for several periods and then were photographed and weighed, respectively.

Biodegradation tests were performed as follows. Six batches of test films (5 × 5 cm^2) enclosed in a nylon mesh netting (2 × 2 mm^2 mesh size) were buried about 25 cm beneath the natural soil. The average values of the temperature, moisture, and pH of the soil were about 25 °C, 25%, and 7.0, respectively. After being buried from 3 to 80 days, the degraded films and fragments were taken out, rinsed with water, and then vacuum-dried at 25 °C for 4 days before the characterizations. The weight loss of the films degraded in soil, w_{loss} (%), was measured and calculated. The half-life $t_{1/2}$ and degradation rate constant k were obtained from double-logarithmic plots of weight loss against the period in soil (t) by the equations given in ref 38.

3. RESULTS AND DISCUSSION

3.1. Structure and Hydrophobicity of RCS Films.
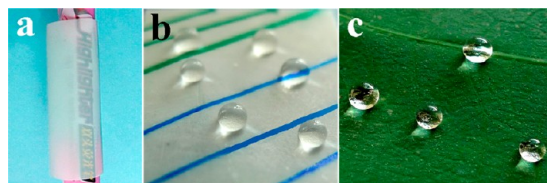Figure 1 shows photographs of the RCS20 composite film and a lotus

Figure 1. Photographs of RCS20 covering on a pen (a), line-drawn with pens (b), and a lotus leaf (c).

leaf. The RCS composite film was very flexible and semi-transparent (Figure 1a) and could be written by pens (Figure 1b). Moreover, the RCS20 exhibited high hydrophobicity, similar to the lotus leaf (Figure 1b,c). So it may also be used in packaging, printing, and coverage such as a keyboard film.

To determine the structure and dispersion of stearic acid on cellulose before hot-pressing, the morphologies of the freeze-dried RCS5−40 gels were studied (Figure S1 in the Supporting Information). Interestingly, some stearic acid micro- and nanosized waxy protrusions appeared on the surface for RCS5, RCS20, and RCS40 (Figure S1a−c in the Supporting Information), indicating the successful incorporation and uniform distribution of stearic acid on the cellulose surface. Figure 2 shows WAXD spectra of RC, RCS5, RCS20, and
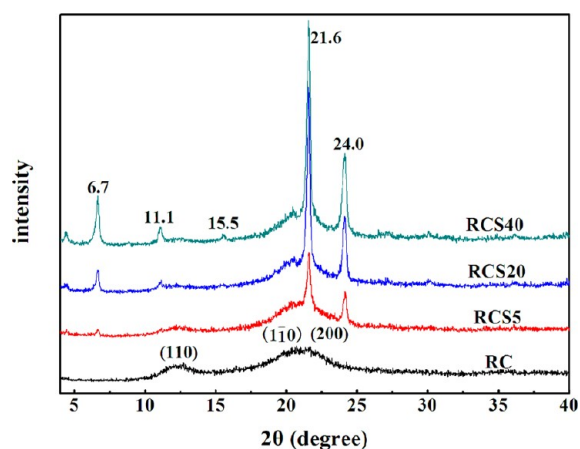

Figure 2. WAXD spectra of RC, RCS5, RCS20, and RCS40.

RCS40. Their crystallinity was calculated to the Lorentz−Gaussian peak separation method[39] to be 49.6, 65.3, 73.4, and 76.1%, respectively. Three crystal peaks at $2\theta = 12°$, $20°$, $21°$ for RC were assigned to crystal planes (110), (1$\bar{1}$0), and (200) of cellulose II, respectively.[40] The peaks at $6.7°$, $21.6°$, and $24.0°$ for RCS corresponded to the interplanar spacings of stearic acid, indicating the stearic acid existed as a crystal form in the RCS composite films. The pure stearic acid crystalline was kept in the RCS films regardless of the cellulose disturbance and the interplanar spacings (d/Å) of the most intense peaks for stearic acid (RCS40) remained.[41] The "long spacing" (0,0,l) of three distinct diffraction peaks at 13.3 (6.7°), 8.0 (11.1°), and 5.7 Å (15.5°) for stearic acid, which were refractions from interplanar spacings (00l) characterized by (003), (005), and (007) indices, respectively, indicating the order and the thickness of molecular layers. Additionally, the

"short spacing" peaks (h,k,0) of 4.1(21.6°) and 3.7 Å (24.0°) appeared at large diffraction angles, showing the hydrocarbon chain lateral packing order.[41,42] These values were assigned to stearic acid monoclinic C-form consistent with the formation crystallized from solution.[43] Interestingly, the stearic acid peaks increased significantly in intensity with an increase of stearic acid content, confirming the presence of the stearic acid crystals in the RCS composite films.

Figure 3 shows the SEM images of the films and water contact angle of each surface. The RC surface was very smooth
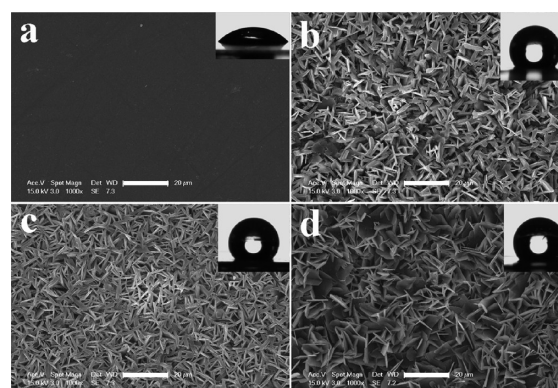

Figure 3. FESEM images of surface for RC (a), RCS5 (b), RCS20 (c), and RCS40 (d) prepared by the hot-pressing dried process (scale bars, 20 μm). Insets show the photographs of the water contact angle on each surface: RC (48.5 ± 0.5°), RCS5 (137.3 ± 1.7°), RCS20 (142.5 ± 1.5°), and RCS40 (145.6 ± 1.2°).

(Figure 3a) and hydrophilic, leading to a low water contact angle value (48.5 ± 0.5°). However, the RCS films treated under the 90 °C and 0.1 MPa hot-pressing exhibited higher water contact angles of more than 137°, indicating a significant improvement in hydrophobicity. Apparently, there was a vast amount of stearic acid platelike crystals on the cellulose surface (Figure 3b−d). The low surface energy stearic acid crystals formed a rough surface on cellulose, and the space among the stearic acid crystals could trap air to improve the hydrophobicity because the water contact angle of air is considered as 180°.[10] Therefore, the trapped air served as part of the surface, and the interface beneath the water drop could be considered as a composite surface. Thus the Cassie model[44,45] can be suitable for this situation, and the equilibrium contact angle θ' can be expressed as

$$\cos \theta' = f \cos \theta + f - 1 \qquad (2)$$

where f and θ are the area fraction and Young angle of the solid in the composite surface.

During the hot pressing process, the ethanol would vaporize and stearic acid stayed melted to disperse well in the cellulose matrix. Then the melted stearic acid formed crystals, and the SA crystals distributed evenly in the cellulose pores, resulting in a rough surface with a space of micro- and nano size. Interestingly, with an increase of the stearic acid concentration, the water contact angle increased, as a result of the increasing of the space amount of the dense layers of stearic acid. To further demonstrate the contribution of stearic acid to the improvement of the hydrophobicity, a filter paper was coated with stearic acid and dyed under the same conditions. The green filter paper floating on water changed to be superhydrophobic (Figure S2 in the Supporting Information), similar to the lotus

leaf. Therefore, the incorporation of stearic acid into cellulose films significantly improved their hydrophobicity.

3.2. Role of SA Crystals on Improvement of the Hydrophobicity. Figure 4 shows the SEM images for the
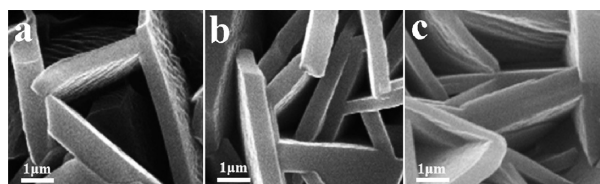

Figure 4. FESEM images of the distribution pattern of stearic acid crystal for RCS5 (a), RCS20 (b), and RCS40(c) films prepared by the hot-pressing dried process.

distributional pattern of stearic acid crystal on cellulose. Clearly, the stearic acid existed as vertical microplate-like crystals on the surface of the RCS5−40 cellulose films. The stearic acid microplates were loosely distributed on the cellulose surface (Figure 4a), which could prevent direct contact between cellulose and the water droplets. For RCS20, the stearic acid microplates were more densely packed together (Figure 4b), resulting in a higher hydrophobicity. Upon further increasing of stearic acid concentration, the layer with similar stearic acid crystals densely packed (Figure 4c), leading to the increasing space amount for the trapping air. Moreover, there were nanostripes appearing on the microplate of the stearic acid crystal surface, indicating a hierarchical structure. The hydrophobicity for RCS40 and RCS20 was better than RCS5 on the whole, as a result of trapping more air. This could be explained that the stearic acid crystals on the surface of RCS20 and RCS40 were smaller and were more densely packed than RCS5, leading to the increase of the space amount. Therefore, the space among stearic acid microplates for trapping air (Cassie state) was the main reason for the higher hydrophobicity.

In our findings, there were many pores in the regenerated gel sheet,[46,47] and the porous structure provided a matrix for stearic acid crystal conservation and growth. The stearic acid crystallization could be induced by the pore wall of cellulose. The stearic acid crystal arranged spontaneously to form a plate-layered structure with space, which existed between the layers. The morphologies of stearic acid microplates on the cellulose surface and the surface as well as the cross-section for stearic acid single crystal were studied (Figure S3 in the Supporting Information). These interesting geometrical caves, such as rhombus-, oval-, and trilateral-like shape (Figure S3a−c in the Supporting Information), could trap air. In addition, there were nano wax protrusions on the cross-section and the surface of stearic acid plates (Figure 4 and Figure S3e,f in the Supporting Information), forming a micronano binary structure. Therefore, the embedding of stearic acid in the cellulose matrix was important to improve the cellulose hydrophobicity, due to low surface energy, the porous surface, and micronano binary structure formation.

To understand the stearic acid crystal growth process, lower stearic acid concentrations were used to fabricate RCS1−3. The SEM images of their surface morphologies are shown in Figure 5. The spheral and rod-shaped stearic acid crystals coexisted in RCS1 with 1% stearic acid concentration (Figure 5a). The Span-80 was used for stearic acid dispersion during the crystal growth process and added into stearic acid ethanol solution to fabricate the RCS3 films with 3% stearic acid concentration
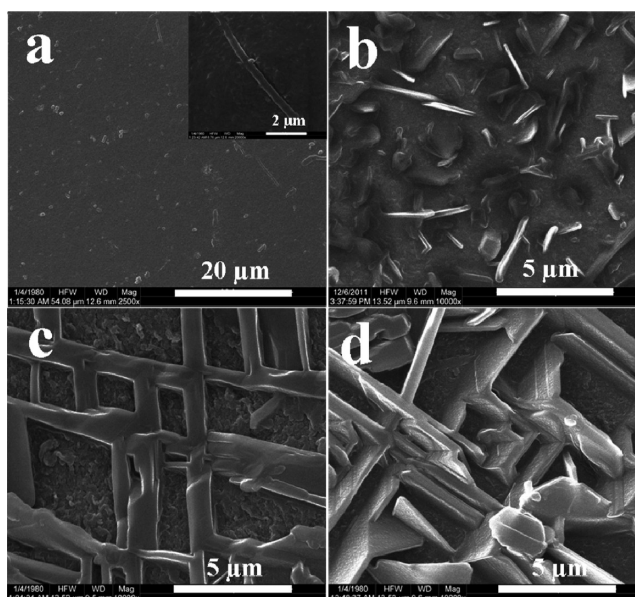

Figure 5. SEM images of surface for RCS1 hot-pressed at 90 °C (a) and RCS3 (b−d) films from different conditions: hot-pressed at 90 °C with 1 wt % of Span 80 (b); hot-pressed at 100 (c) and 90 °C (d), respectively. The inset in part a is its enlargement.

(Figure 5b).[48] It was noted that these stearic acid crystals showed rod-shaped and a microplate crystal (Figure 5b−d), and mostly grew forward continuously without packed space. It was not hard to imagine that when the stearic acid was very little and the space of the cellulose pores was relative large, the stearic acid spheres could be assembled to form a rod shaped crystal, considering the evidence of nanowax protrusions on a stearic acid microplate (Figure S3e,f in the Supporting Information). Moreover, the temperature could govern the shrinking rate of cellulose pores and the kinetics of crystallization.[49] The rod-shaped stearic acid crystal occurred on RCS3 hot-pressed at 100 °C (Figure 5c) rather than vertical microplate-like crystal at 90 °C (Figure 5d). This was as a result of the relatively small pore for the stearic acid crystal growth process induced by the relatively high temperature and ethanol vaporization velocity, which led to the shrinking of cellulose pores. Therefore, the porous structure of the cellulose matrix could lead to the formation of layered or rod-shaped crystals. The relatively large pores mainly resulted in the microplate crystal formation. Moreover, these pores could effectively control stearic acid crystal homogeneous dispersion and restrict growth, leading to the crystals that became smaller in size but the space amount increased. The stearic acid crystal growth process may be described as follows: the spherical stearic acid crystals formed initially when the pore space of cellulose was large and they could assemble into rod-shaped and vertical microplate-like crystals in the relatively smaller pore space depending on the hot-pressing temperatures. Therefore, the stearic acid crystal could be controlled by adjusting the relative pore size of cellulose through stearic acid concentration, hot-pressed temperature, and the addition of surfactant.

The stearic acid crystal morphologies obtained at different temperatures may be related also to their thermal properties, so DSC was employed to study the melting temperature and crystallization behavior of the samples (Figure 6). An endothermic peak was found around 68.3 °C for RCS, which was clearly below that of stearic acid at 71.0 °C. The shift of the
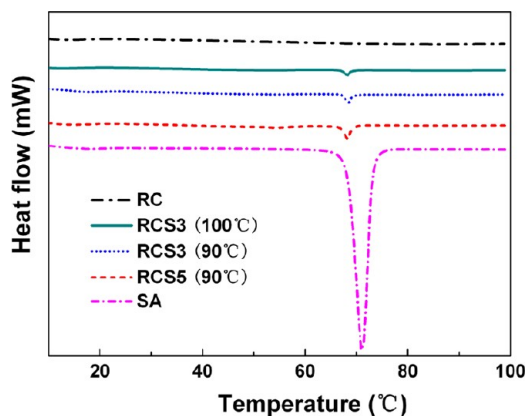
Figure 6. DSC heating curves of the RC, RCS hot-pressed at 100 and 90 °C, and stearic acid. Scanning rate 5 °C/min.

endothermic peak for RCS to lower temperature further indicated that the cellulose pores induced the stearic acid crystal growth, leading to the decrease of T_m for stearic acid. Additionally, the melting enthalpy for RCS3 hot-pressed at 100 and 90 °C were 2.754 and 4.194 J/g, respectively, indicating the distinct and more ordered stearic acid crystal structure at 90 °C.[48]

Furthermore, the FT-IR and solid-state ^{13}C NMR spectra of the RC and RCS films (Figure S4 in the Supporting Information) indicated that only physical interactions existed between stearic acid and cellulose and no chemical reaction occurred during the hot-pressing process between them (see details in the Supporting Information).

3.3. Physical Properties and Biodegradability of RCS Films. Figure 7 shows the mechanical properties of the composite films in the dry and the humid states. The RCS films in the dry state exhibited good tensile strength (σ_b) and higher elongations at the break (ε_b) than RC. The σ_b and ε_b values of the RCS films in the humid state (Figure 7b) were both higher than that of RC due to the moisture-proof ability of the stearic acid layer and the stearic acid plasticization effect. These results indicated a successful improvement in water resistance and mechanical properties of RC in the humid state. Clearly, the mechanical properties of RCS were much better than ordinary paper such as copy paper (CP) and thermal paper (TP) in the dry and humid state. The moisture resistibility (W_R) could be calculated according to eq 3 as follows:

$$W_R(\%) = \frac{\sigma_{at\ humid}}{\sigma_{at\ dry}} \times 100\% \qquad (3)$$

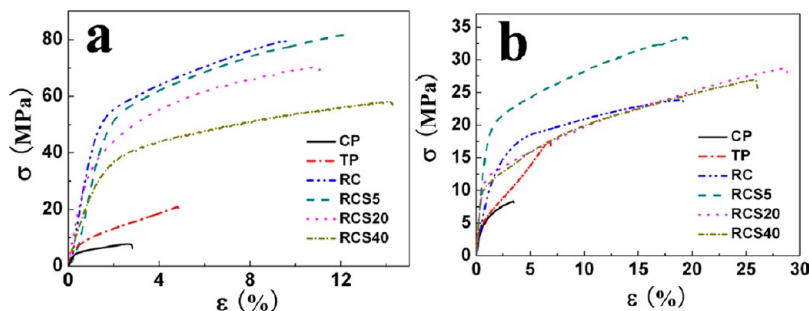The W_R for RC was 30%, lower than that of RCS, and the W_R values for RCS5–40 were 41%, 41.5%, and 46.4%, respectively, indicating significant improvement of W_R.

To further investigate the water-resistance of RCS5–40 and RC films, the films were soaked in water and the dynamic water uptake plot was measured. The water uptake of the composite films and RC immersed in distilled water is shown in Figure 8.
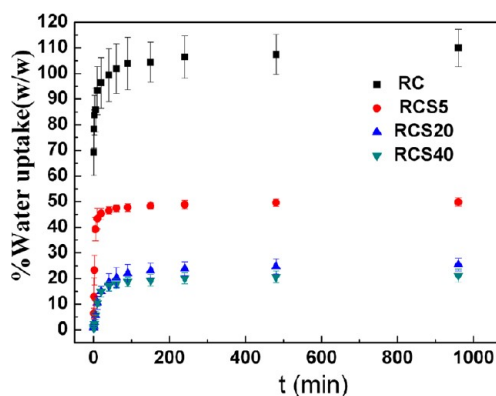

Figure 8. Water uptake of the films immersed in distilled water.

For RC, the saturated water uptake ratio can reach 108% (Figure 8). As is predicted, the incorporation of stearic acid can reduce the water uptake ratio because of the water-resistant buffering effect of the stearic acid layer. Moreover, this effect became more significant with an increase of the stearic acid concentration, and the saturated water uptake ratio for RCS5, RCS20, and RCS40 was 50%, 25%, and 20%, respectively (Figure 8, RCS5–40). Therefore, the water-resistance ability was improved greatly as a result of the presence of the micronano binary structure.

Figure 9 shows the photographs of mung beans stored in vessels with RC (parts a–c) and RCS20 (parts d–f) as the bottom for different periods at 25 °C and the time dependence of the weight increase for the beans (Figure 9, right). Obviously, the mung beans on RC became swollen and germinated after 36 h, and the weight of mung beans increased gradually with the test time, indicating the poor water resistant properties of RC. However, the beans on RCS20 remained intact, and the weights at different times changed hardly, so the RCS20 exhibited much better water resistant properties than RC. The stearic acid layer cannot only prevent the direct contact between water and cellulose but can also prevent the contact between beans and cellulose, resulting in good water resistant properties. Therefore, the RCS20 has potential to be used in waterproof package materials.
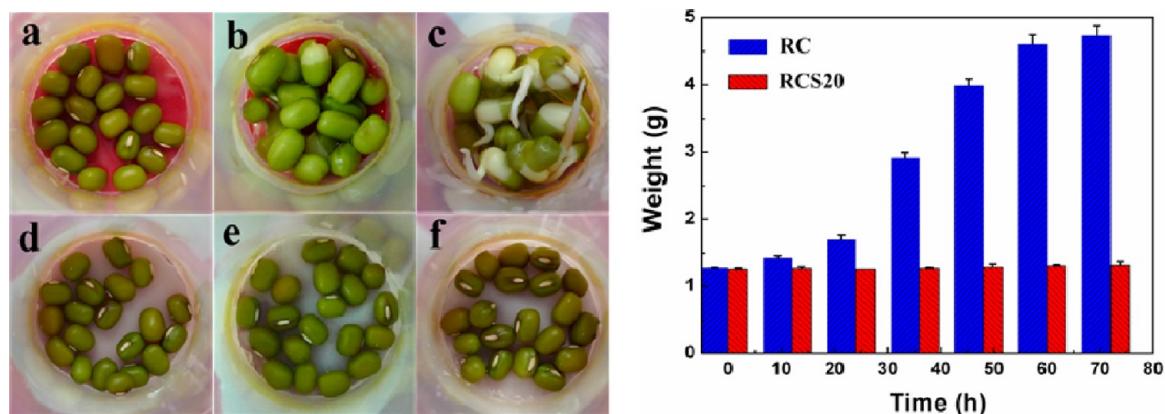

Figure 7. Stress–strain (σ–ε) curves of CP, TP, RC, RCS5, RCS20, and RCS40 films in the dry state (a) and the humid state (b) at 25 °C.

Figure 9. Photographs of mung beans stored in vessels with RC (a−c) and RCS20 (d−f) as the bottom for 0 (a,d), 24 (b,e), and 36 h (c,f) at 25 °C, respectively, (left) and the time dependence of the weight increase for the beans (right).
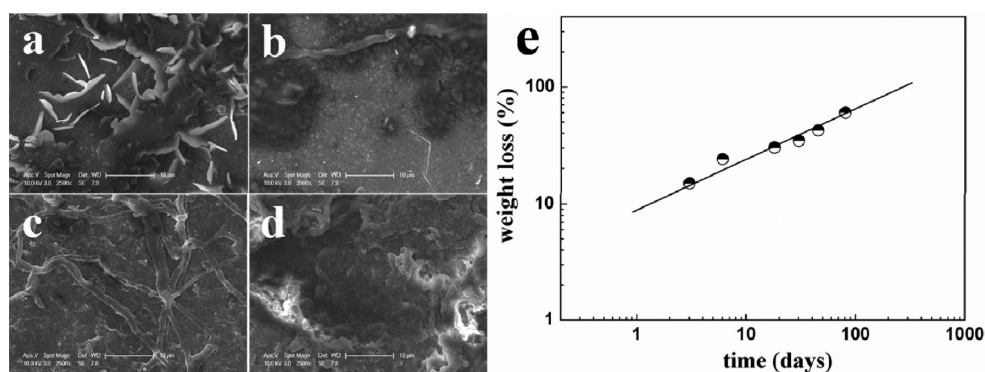

Figure 10. FESEM images of the RCS20 surface degraded for (a) 6 days, (b) 18 days, (c) 30 days, and (d) 45 days and the dependence of weight loss on the degradation time for RCS20 in soil at 25 °C (e).

SEM images of the RCS20 film biodegraded in the soil for 6 days (a), 18 days (b), 30 days (c), and 45 days (d) are shown in Figure 10. There was still stearic acid plate crystal left on the cellulose surface after being buried for 6 days in the soil (Figure 10a). However, after 18 days of degradation (Figure 10b), the stearic acid almost vanished and some fungal mycelia began to appear on the surface of the decayed film. Clearly, the biodegradation of the RCS20 was caused by the microorganisms in the soil, and this process occurred gradually. After having been buried in the soil for 30 days, large amount of fungal mycelia appeared on the surface (Figure 10c), and the microorganisms in the soil directly attacked and metabolized the cellulose. Furthermore, only broken fragments of the film were observed after 45 days (Figure 10d), and the surface became bumpy due to the metabolization. Figure 10e shows the plot for the biodegradable kinetics of the RCS20 film in the soil. The half-life $t_{1/2}$ obtained from double-logarithmic plots of weight loss against the burying period in soil (t) was 52 days, and the biodegradation rate constant (k) was 0.43. The results revealed that the RCS20 film could be biodegraded completely in 250 days. Therefore, the cellulose based material fabricated via the simple and "green" process is safe and biodegradable.

4. CONCLUSIONS

A novel, highly hydrophobic and biodegradable regenerated cellulose film RCS embedded with stearic acid was successfully prepared through the solvent-vaporized crystallization. The stearic acid crystals were encaged in the pores of the cellulose matrix, and the controllable stearic acid crystallization was induced by the pore wall to form a micronano binary structure, resulting in better ability to trap abundant air for the improvements in the hydrophobicity. The RCS films exhibited high hydrophobicities, good water-resistance properties, and biodegradability. The stearic acid crystals played an important role in the improvement of hydrophobicities for the cellulose film, as a result of the formation of a rough surface with a hierarchical structure indicating micronano space on the film. Therefore, the RCS films were highly hydrophobic, biodegradable, safe, and inexpensive, showing great potential in applications in biodegradable waterproof packaging.

■ ASSOCIATED CONTENT

Ⓢ Supporting Information

SEM images of films from the freezing-dried process and the morphologies of stearic acid microplates on the surface of the films (Figures S1 and S3), the FT-IR spectra (A) and solid-state ^{13}C NMR (B) of the films (Figure S4), and a photograph as well as SEM images of a superhydrophobic filter paper (Figure S2). This material is available free of charge via the Internet at http://pubs.acs.org.

■ AUTHOR INFORMATION

Corresponding Author

*Phone: +86-27-87219274. Fax: +86-27-68762005. E-mail: lnzhang@public.wh.hb.cn.

Notes

The authors declare no competing financial interest.

590

dx.doi.org/10.1021/am3026536 | ACS Appl. Mater. Interfaces 2013, 5, 585−591

■ REFERENCES

(1) Bitinis, N.; Hernandez, M.; Verdejo, R.; Kenny, J. M.; Lopez-Manchado, M. A. *Adv. Mater.* **2011**, *23*, 5229−5236.

(2) Zhang, Q.; Zhang, S.; Deng, Y. *Green Chem.* **2011**, *13*, 2619−2637.

(3) Cai, J.; Zhang, L.; Liu, S.; Liu, Y.; Xu, X.; Chen, X.; Chu, B.; Guo, X.; Xu, J.; Cheng, H. *Macromolecules* **2008**, *41*, 9345−9351.

(4) Chang, C.; Chen, S.; Zhang, L. *J. Mater. Chem.* **2011**, *21*, 3865−3871.

(5) Qi, H.; Chang, C.; Zhang, L. *Green Chem.* **2008**, *11*, 177−184.

(6) Luo, X.; Liu, S.; Zhou, J.; Zhang, L. *J. Mater. Chem.* **2009**, *19*, 3538−3545.

(7) Chang, C.; He, M.; Zhou, J.; Zhang, L. *Macromolecules* **2011**, *44*, 1642−1648.

(8) Cai, J.; Zhang, L.; Zhou, J.; Qi, H.; Chen, H.; Kondo, T.; Chen, X.; Chu, B. *Adv. Mater.* **2007**, *19*, 821−825.

(9) Feng, L.; Li, S.; Li, Y.; Li, H.; Zhang, L.; Zhai, J.; Song, Y.; Liu, B.; Jiang, L.; Zhu, D. *Adv. Mater.* **2002**, *14*, 1857−1860.

(10) Jiang, L.; Zhao, Y.; Zhai, J. *Angew. Chem., Int. Ed.* **2004**, *116*, 4438−4441.

(11) Lai, Y.; Gao, X.; Zhuang, H.; Huang, J.; Lin, C.; Jiang, L. *Adv. Mater.* **2009**, *21*, 3799−3803.

(12) Erbil, H. Y.; Demirel, A. L.; Avcı, Y.; Mert, O. *Science* **2003**, *299*, 1377.

(13) Zhao, N.; Weng, L.; Zhang, X.; Xie, Q.; Xu, J. *ChemPhysChem* **2006**, *7*, 824−827.

(14) Lai, H. M.; Padua, G. W. *Cereal Chem.* **1997**, *74*, 771−775.

(15) Raj, R.; Kokta, B.; Dembele, F.; Sanschagrain, B. *J. Appl. Polym. Sci.* **1989**, *38*, 1987−1996.

(16) Wu, T.; Pan, Y.; Li, L. *J. Colloid Interface Sci.* **2010**, *348*, 265−270.

(17) Theneshkumar, S.; Gnanaprakash, D.; Nagendra Gandhi, N. *J. Chem. Eng. Data* **2010**, *55*, 2980−2984.

(18) Shepherd, T.; Robertson, G.; Griffiths, D.; Birch, A.; Duncan, G. *Phytochemistry* **1995**, *40*, 407−417.

(19) Sebti, I.; Ham-Pichavant, F.; Coma, V. *J. Agric. Food Chem.* **2002**, *50*, 4290−4294.

(20) Lodha, P.; Netravali, A. N. *Ind. Crops Prod.* **2005**, *21*, 49−64.

(21) Nyfors, L.; Suchy, M.; Laine, J.; Kontturi, E. *Biomacromolecules* **2009**, *10*, 1276−1281.

(22) Taajamaa, L.; Kontturi, E.; Laine, J.; Rojas, O. J. *J. Mater. Chem.* **2012**, *22*, 12072−12082.

(23) Berlioz, S.; Molina-Boisseau, S.; Nishiyama, Y.; Heux, L. *Biomacromolecules* **2009**, *10*, 2144−2151.

(24) Wang, J.; Somasundaran, P. *J. Colloid Interface Sci.* **2006**, *293*, 322−332.

(25) Ding, B.; Li, C.; Hotta, Y.; Kim, J.; Kuwaki, O.; Shiratori, S. *Nanotechnology* **2006**, *17*, 4332.

(26) Balu, B.; Breedveld, V.; Hess, D. W. *Langmuir* **2008**, *24*, 4785−4790.

(27) Cunha, A. G.; Freire, C. S. R.; Silvestre, A. J. D.; Neto, C. P.; Gandini, A.; Orblin, E.; Fardim, P. *Biomacromolecules* **2007**, *8*, 1347−1352.

(28) Jonoobi, M.; Harun, J.; Mathew, A. P.; Hussein, M. Z. B.; Oksman, K. *Cellulose* **2010**, *17*, 299−307.

(29) Cunha, A. G.; Freire, C.; Silvestre, A.; Neto, C. P.; Gandini, A.; Belgacem, M. N.; Chaussy, D.; Beneventi, D. *J. Colloid Interface Sci.* **2010**, *344*, 588−595.

(30) Bayer, I. S.; Fragouli, D.; Attanasio, A.; Sorce, B.; Bertoni, G.; Bresica, R.; Corato, R.; Pelegrino, T.; Kalyva, M.; Sabella, S. *ACS Appl. Mater. Interfaces* **2011**, *3*, 4024−4031.

(31) Herminghaus, S. *Europhys. Lett.* **2000**, *52*, 165.

(32) Gao, X.; Jiang, L. *Nature* **2004**, *432*, 36−36.

(33) Joung, Y. S.; Buie, C. R. *Langmuir* **2011**, *27*, 4156−4163.

(34) Zhang, D.; Yu, W.; Hao, D.; Li, L.; Liu, H.; Lu, Z. L. *J. Mater. Chem.* **2012**, *22*, 17328−17331.

(35) Meng, T.; Xie, R.; Ju, X.; Cheng, C.; Wang, S.; Li, P.; Liang, B.; Chu, L. *J. Membr. Sci.* **2013**, *427*, 63−72.

(36) Feng, X.; Jiang, L. *Adv. Mater.* **2006**, *18*, 3063−3078.

(37) Cai, J.; Liu, Y.; Zhang, L. *J. Polym. Sci., Part B: Polym. Phys.* **2006**, *44*, 3093−3101.

(38) Zhang, L.; Liu, H.; Zheng, L.; Zhang, J.; Du, Y.; Feng, H. *Ind. Eng. Chem. Res.* **1996**, *35*, 4682−4685.

(39) Rabek, J. F. In *Experimental Methods in Polymer Chemistry*. Wiley-Interscience: Chichester, U.K., 1980; Vol. *1*, p 507.

(40) Isogai, A.; Usuda, M.; Kato, T.; Uryu, T.; Atalla, R. H. *Macromolecules* **1989**, *22*, 3168−3172.

(41) Teixeira, A. C. T.; Garcia, A. R.; Ilharco, L. M.; Gonçalves da Silva, A. M. P. S.; Fernandes, A. C. *Chem. Phys. Lipids* **2010**, *163*, 655−666.

(42) Ensikat, H.; Boese, M.; Mader, W.; Barthlott, W.; Koch, K. *Chem. Phys. Lipids* **2006**, *144*, 45−59.

(43) Malta, V.; Celotti, G.; Zannetti, R.; Martelli, A. F. *J. Chem. Soc. B* **1971**, 548−553.

(44) Cassie, A.; Baxter, S. *Trans. Faraday Soc.* **1944**, *40*, 546−551.

(45) Crick, C. R.; Parkin, I. P. *Chem.—Eur. J.* **2010**, *16*, 3568−3588.

(46) Chang, C.; Peng, J.; Zhang, L.; Pang, D. W. *J. Mater. Chem.* **2009**, *19*, 7771−7776.

(47) Liu, S.; Zhang, L.; Zhou, J.; Xiang, J.; Sun, J.; Guan, J. *Chem. Mater.* **2008**, *20*, 3623−3628.

(48) Severino, P.; Pinho, S. C.; Souto, E. B.; Santana, M. H. A. *Colloids Surf. B* **2011**, *86*, 125−130.

(49) Sala, S.; Elizondo, E.; Moreno, E.; Calvet, T.; Cuevas-Diarte, M. A.; Ventosa, N.; Veciana, J. *Cryst. Growth Des.* **2010**, *10*, 1226−1232.